Petroleum Science 19 (2022) 1592–1604

Contents lists available at ScienceDirect

Petroleum Science

journal homepage: www.keaipublishing.com/en/journals/petroleum-science

Original Paper

Fluid discrimination incorporating amplitude variation with angle inversion and squirt flow of the fluid

Yu-Rong Wang [a, b, c], Zhao-Yun Zong [a, b, c, *], Xing-Yao Yin [a, b, c]

[a] China University of Petroleum, Qingdao, Shandong, 266580, China
[b] Shandong Provincial Key Laboratory of Deep Oil and Gas, Qingdao, Shandong, 266580, China
[c] Pilot National Laboratory for Marine Science and Technology (Qingdao), Shandong, 266580, China

ARTICLE INFO

Article history:
Received 22 June 2020
Accepted 26 September 2021
Available online 4 March 2022

Edited by Jie Hao

Keywords:
Fluid discrimination
Poroelasticity theory
Linearized seismic reflectivity
Pre-stack seismic inversion
Squirt flow of fluid

ABSTRACT

Pre-stack seismic inversion is an important method for fluid identification and reservoir characterization in exploration geophysics. In this study, an effective fluid factor is initially established based on Biot poroelastic theory, and a pre-stack seismic inversion method based on Bayesian framework is used to implement the fluid identification. Compared with conventional elastic parameters, fluid factors are more sensitive to oil and gas. However, the coupling effect between rock porosity and fluid content is not considered in conventional fluid factors, which may lead to fuzzy fluid identification results. In addition, existing fluid factors do not adequately consider the physical mechanisms of fluid content, such as squirt flow between cracks and pores. Therefore, we propose a squirt fluid factor (SFF) that minimizes the fluid and pore mixing effects and takes into account the squirt flow. On this basis, a novel P-wave reflection coefficient equation is derived, and the squirt fluid factor is estimated by amplitude variation with offset (AVO) inversion method. The new reflection coefficient equation has sufficient accuracy and can be utilized to estimate the parameters. The effectiveness and superiority of the proposed method in fluid identification are verified by the synthetic and field examples.

1. Introduction

Fluid identification has always been a hot topic in seismic exploration. Reliable fluid identification can improve the exploration success rate and reduce the investment cost, which is of great significance to oil and gas exploration and reservoir evaluation. Seismic fluid identification mainly includes two parts, one is the construction of fluid indicators, the other is the extraction of fluid indicators from seismic data. Direct indicators such as bright and non-bright spots have been widely used in reservoir characterization (Mazzotti, 1990; Ross and Kingman, 1995; Zdanowski and Górniak, 2014; Wojcik et al., 2016). However, these fluid indicators are very sensitive to any fluid saturation, which will make the interpretation results ambious (Allen et al., 1993; Myśliwiec, 2004; Cichostępski et al., 2019). Certain fluid changes can have substantial effects on bright spots and AVO analysis (Batzle et al., 1995). Therefore, it is necessary to extend the definition of hydrocarbon indicator to fluid classification. The construction of conventional fluid factors was originally derived from the elastic parameters of the simplified Zoeppritz equation (Zoeppritz and Erdbebenwellen, 1919) and extracted from pre-stack seismic data. Smith and Gidlow (1987) defined the fluid factor and developed a weighted stacking method for gas reservoir detection using the amplitude variations with offset (AVO) theory. By studying the tensile properties of underground strata, Goodway et al. (1997) discovered a new fluid factor $\lambda\rho$ and $\mu\rho$ (Lame parameters $\times$ density) to identify the fluid type of the reservoir. Based on the pore elasticity theory of porous elastic medium, Russell et al. (2003) defined ρf to reflect the pore fluid type. Russell et al. (2011) further defined the Gassmann fluid terms f as a fluid factor and extended the linearized AVO approximation. Due to the mixing effect of fluid and pore, these fluid indicators have the solid-liquid coupling fluid identification illusion problems. Yin and Zhang (2014) proposed a new AVO approximate reflectivity equation to estimate the effective pore-fluid bulk modulus, avoiding the strong nonlinearity between seismic data and fluid bulk modulus. Zong et al. (2015) introduced a new linear P-wave reflection coefficient

* Corresponding author. China University of Petroleum, Qingdao, Shandong, 266580, China.
E-mail address: zongzhaoyun@upc.edu.cn (Z.-Y. Zong).

https://doi.org/10.1016/j.petsci.2022.03.007

equation in terms of fluid modulus (FM). FM was affected only by fluids and not by physical properties of rocks such as porosity. Based on the classical fluid indicator, Zhang et al. (2016) constructed a new fluid indicator by considering the squirt flow effect between rock pores and cracks. In addition, different unconventional fluid indication construction methods and corresponding fluid identification strategies were proposed. Shaw and Sen (2006) presented a method for estimating fluid indicators using full-azimuth AVOA (amplitude-versus-offset-and-azimuth) data. Liu and Ghosh (2017), based on the Gassmann-Biot theory, proposed a new seismic attribute J to reduce the uncertainty of oil and gas prediction in the case of different porosity.

The squirt flow mechanism that causes seismic wave attenuation and velocity dispersion contains the relevant information of fluid and skeleton in the actual reservoir. The introduction of squirt flow in fluid discrimination can reduce the false bright spots and the uncertainty of seismic exploration (Barak et al., 2018). The conventional fluid factor is only based on the assumption of uniform pore distribution and neglects the effect of the “local flow” action on the pore scale (O'Connell and Budiansky, 1977). Underground rock media contains a large number of pores and cracks, which are essential for the occurrence of oil and gas (Wu et al., 2015; Kumar et al., 2018, 2019; Kumari et al., 2021; Kumari and Kumar, 2020). When pores and cracks coexist, the aspect ratio of crack is much smaller than that of pore. Under the action of external stress, the pore fluid will be squeezed from cracks into pores and this local flow is called “squirt flow”. This squirt flow is considered to be an important cause of velocity dispersion and energy attenuation of seismic wave in fluid-bearing rocks (Mavko and Nur, 1975; Murphy et al., 1986; Wojcik et al., 2016; Zong and Wang, 2019). Tang (2011) analyzed the squirt effect in detail and proposed a unified theory of elastic wave propagation. On basis of the unified theory, a kind of squirt fluid factor (SFF) considering the squirt flow is established to improve the precision of fluid discrimination.

Seismic inversion method is an important tool for accurately estimating fluid factor from seismic reflection data (Shuey, 1985; Downton, 2005; Skopintseva et al., 2011; Kumari et al., 2017; Li et al., 2020; Kumar and Kumari, 2020). According to the approximate orders and optimization methods of reflection coefficient equation, seismic inversion can be divided into nonlinear and linear AVO inversion. Nonlinear AVO inversion is based on the exact or high-order reflection coefficient equation (Gholami et al., 2018). Yin et al. (2016) used the high-order Zoeppritz approximation equation to solve AVO problems in the trust region by applying the inverse operator estimation algorithm. In order to overcome the non-uniqueness problem, Mollajan et al. (2019) used imperialist competitive algorithm optimization method to solve nonlinear AVO inversion. Linear AVO inversion methods are generally based on linear reflection coefficient equation. Although AVO linear approximation equation is limited to approximation conditions, it plays an important role in fluid identification due to its efficiency and stability (Downton and Ursenbach, 2006; Tor et al., 2008). The Bayesian formula establishes the quantitative relationship between the posterior probability distribution of model parameters and the prior distribution and likelihood function (Dashti and Stuart, 2016; Lang and Grana, 2018; Zhang et al., 2019). Prior distribution can be selected according to the actual situation, such as Huber distribution, Cauchy distribution, Gauss distribution, etc. Compared with the conventional Gaussian probability distribution, Cauchy distribution has long tails and could generate sparse solutions (Zhang et al., 2018). Therefore, Cauchy distribution is selected as the prior information of inversion to make the inversion results more stable and high-resolution.

In this study, we focus on the construction approach of fluid factors and the prediction approach of the fluid factor from pre-stack seismic data. A fluid discrimination approach method combining the unified theory of porous media with cracks and Bayesian AVO inversion is proposed. Firstly, we start by building a squirt fluid factor (SFF) based on a unified theory. The squirt flow due to the uneven distribution of pores and cracks will cause deviation of fluid identification, and the squirt fluid factor (SFF) can take the effect of squirt flow into consideration. Secondly, we derive a novel reflection coefficient in terms of SFF. Finally, the parameters are solved in the Bayesian frame for the higher stability and accuracy. The application of model and field data demonstrates the robustness and effectiveness of the proposed method.

2. A cracked porous medium elastic wave theory

The rock medium usually contains both pores and cracks, which have an important effect on the elastic wave propagation. On the basis of Biot's poroelastic wave theory, Tang (2011, 2012) introduced the influence of cracks and proposed a unified elastic wave theory. The cracked porous medium wave theory can simulate the attenuation and dispersion of elastic wave caused by squirt flow. And crack density and aspect ratio are introduced as two important parameters to describe porous rocks with cracks.

For a porous rock modeled by Biot's theory, the mass conservation of fluid in porous rock follows

$$\frac{\partial\left(\rho_{\mathrm{f}}\varphi\right)}{\partial t}+\frac{\partial\left[\rho_{\mathrm{f}}\varphi(U_t-u_t)\right]}{\partial x\partial t}=0 \tag{1}$$

The porosity differential is related to the skeleton deformation difference, and the density difference is related to the fluid pressure.

$$\frac{\partial\varphi}{\partial t}=a\frac{\partial^2 u}{\partial x\partial t}+\frac{1}{Q}\frac{\partial P}{\partial t} \tag{2}$$

$$\frac{\partial\rho_{\mathrm{f}}}{\partial t}=\frac{1}{c_0^2}\frac{\partial P}{\partial t} \tag{3}$$

where

$$a=1-\frac{K_{\mathrm{d}}}{K_{\mathrm{s}}}$$

$$\frac{1}{Q}=\frac{1}{K_{\mathrm{s}}}\left(1-\varphi-\frac{K_{\mathrm{d}}}{K_{\mathrm{s}}}\right)$$

By substituting Eqs. (2) and (3) into Eq. (1), we can get the relationship between fluid pressure and displacements.

$$P=-\left(au_x+\varphi(U_x-u_x)\right)/F \tag{4}$$

$$F=\frac{\varphi}{K_{\mathrm{f}}}+\frac{1}{Q}$$

where U is fluid displacement, u is solid displacement, ρ_{f} is fluid density, φ is porosity, P is pore fluid pressure, subscripts x and t indicate partial derivatives, c_0 is acoustic velocity in fluid, K_{d} is dry bulk modulus of the solid, K_{s} and K_{f} is the bulk modulus of the solid grain and of the pore fluid respectively.

Tang et al. (2012) introduces cracks into the porous rock and squirt flow between cracks and pores occurs. The pore fluid pressure is affected by the squirt flow, which depends on the amount of fluid flowing into and out of the pore space. In the porous rock containing flat- or narrow-shaped cracks, the pore fluid pressure is

$$P = -(au_x + \varphi(U_x - u_x) + \varphi q_v)/F \tag{5}$$

The squirt flow effect can be characterized as,

$$S(\omega) = \varphi q_v / P \tag{6}$$

By substituting $S(\omega)$ into Eq. (4), the pore fluid pressure becomes,

$$P = -(au_x + \varphi(U_x - u_x) + \varphi q_v)/(F + S(\omega)) \tag{7}$$

$$S(\omega) = \frac{8\varepsilon(1-\sigma)(1+\lambda)^3}{3\mu} \times \frac{\left(\frac{1/K_g - 1/K_s}{1/K_d - 1/K_g}\right)M}{1 - \frac{3i\omega\eta(1+2\lambda)}{2K_f\lambda\gamma^2}\left[1 + \frac{4(1-\sigma)K_f(1+\lambda)^3}{3\pi\mu\gamma(1+2\lambda)}M\right]} \tag{8}$$

$$M = 1 + \frac{4-5\sigma}{2(7-5\sigma)}\frac{\lambda^3}{(1+\lambda)^3} + \frac{9}{2(7-5\sigma)}\frac{\lambda^5}{(1+\lambda)^5} \tag{9}$$

$$\lambda = \left(\frac{3\varphi}{4\pi\varepsilon}\right)^{1/3}$$

In a unit volume of rock, the increment of fluid expansion in pore space caused by local fluid flow is q_v. η is viscosity coefficient, ε is crack density, μ, σ and K_g are shear modulus, Poisson's ratio and bulk modulus of background medium in the absence of squirt flow. $\omega = 2\pi fre$ is angular frequency, fre is dominant frequency of seismic in the work area.

3. The extension of poroelastic theory

In the Biot theory, there are three kinds of waves that can propagate in fluid-filled porous media, fast compressional wave, shear wave and slow compressional wave. Fast compressional wave and shear wave are mainly related to the elasticity of solid skeleton and pore fluid. Slow compressional wave is affected by the fluid and skeleton motion (Biot, 1956a, b). The main factors affecting seismic reflection characteristics include the velocity of seismic wave and density of medium. And the situation becomes more complicated when medium contains pore and fluid. The effects of fluid saturation can be described by Gassmann equation. According to the poroelastic theory, the P-velocity V_p and S-velocity V_s under the low frequency condition are defined as,

$$V_p = \sqrt{\frac{K_{sat} + \frac{4}{3}\mu}{\rho_{sat}}},\ V_s = \sqrt{\frac{\mu}{\rho_{sat}}} \tag{10}$$

$$K_{sat} = K_d + \frac{\left(1 - \frac{K_d}{K_s}\right)^2}{\frac{\varphi}{K_f} + \frac{1-\varphi}{K_s} - \frac{K_d}{K_s^2}},\ \mu = \mu_d \tag{11}$$

where K_{sat}, K_s, K_d and K_f are the bulk modulus of fluid-saturated rock, rock matrix, dry rock, and the saturated fluid respectively. φ, μ and ρ_{sat} are effective porosity, shear modulus and density respectively. Russell fluid factor f is defined as,

$$f = \frac{\left(1 - \frac{K_d}{K_s}\right)^2}{\frac{\varphi}{K_f} + \frac{1-\varphi}{K_s} - \frac{K_d}{K_s^2}} = \alpha^2 N \tag{12}$$

$$K_{sat} = K_d + f \tag{13}$$

$$\alpha = 1 - \frac{K_d}{K_s} \tag{14}$$

$$\frac{1}{N} = \frac{\alpha - \varphi}{K_s} + \frac{\varphi}{K_f} \tag{15}$$

where α is Biot coefficient, N is a certain modulus.

According to Voigt bound, it is reasonable to assume that at high porosity (Batzle, 2004),

$$0 \le 1 - \varphi - \frac{K_d}{K_0} << \varphi\frac{K_d}{K_s} \tag{16}$$

By simplifying Eq. (12), Russell fluid factor f can be expressed as,

$$f = \frac{\left(1 - \frac{K_d}{K_s}\right)^2}{\frac{\varphi}{K_f}} = \alpha^2 N = \frac{\alpha^2}{\varphi}K_f \tag{17}$$

From Eq. (12) we can know that Russell fluid factor f is not only affected by fluid but also the dry rock bulk modulus, rock matrix modulus and porosity. However, porosity easily causes considerable ambiguity in fluid identification (Yu et al., 1993). Therefore, it's necessary to diminish the porosity impact on fluid indicator and reduce ambiguity.

The Biot-consistent theory introduce the effect of crack by K_d,

$$K_d = \mu_d\frac{2 + 2\sigma_d}{3 - 6\sigma_d} \tag{18}$$

where μ_d and σ_d are the shear modulus and Poisson's ratio of solid grains respectively. And σ_d must be calculated in an iteration scheme based on the Biot-consistent theory (Thomsen, 1985).

$$\mu_d = \mu_s\left(1 - \frac{\varphi}{1-p} - q\varepsilon\right) \tag{19}$$

$$\varepsilon = \frac{3}{4\pi}\frac{\varphi_c}{\gamma} \tag{20}$$

In Eq. (19), ε is crack density, φ_c is volume fraction of crack, γ is aspect ratio of crack, μ_s is shear modulus of matrix. Substituting K_d of Eq. (18) into Eq. (11) and we can describe the influence of pores and cracks on the elastic properties of media. However, to extend this influence into frequency domain, we must take the squirt flow effect into consideration.

According to the derivation of Gassmann formula, Tang (2011) proposed a new rock physical equation which maintains both the basic characteristics and structure of Biot theory (Eq. (21)). Compared to Eq. (11), Eq. (21) adds a contribution item $S(\omega)$ to characterize the squirt flow. We define $S(\omega)$ as a term representing the contribution of the squirt flow and define S as a total squirt flow effect item.

$$K_{sat} = K_d + \frac{\left(1 - \frac{K_d}{K_s}\right)^2}{\frac{\varphi}{K_f} + \frac{1-\varphi}{K_s} - \frac{K_d}{K_s^2} + S(\omega)} \tag{21}$$

K_f in this equation uses water's bulk modulus. Eq. (21) can be simplified as,

$$K_{sat} = K_d + \frac{\alpha^2 N}{1 + S(\omega)N} = K_d + \frac{f}{1 + S(\omega)N} \tag{22}$$

$$f_s = \frac{f}{S},\ S = 1 + S(\omega)N \tag{23}$$

By incorporating total squirt flow effect item and Russell fluid factor, f_s is generated (Zhang et al., 2016). It retains the original characteristics and structure of the conventional fluid factor and also reflects the influence of the squirt flow effect on the wave propagation. However, to diminish porosity impact on fluid indicator, we further establish a solid - liquid decoupling fluid factor considering squirt flow effect (SFF).

Referring to Eq. (17),

$$f_s = \frac{\alpha^2}{\varphi}\frac{K_f}{S} \tag{24}$$

$$f_s = \frac{\alpha^2}{\varphi}K_{fs} \tag{25}$$

$$K_{fs} = \frac{K_f}{S} \tag{26}$$

K_{fs} is the proposed squirt fluid factor (SFF). We generate K_{fs} by incorporating total squirt flow effect item S and fluid modulus K_f. The new factor reflects the comprehensive response of fluid modulus and squirt flow in the form of elastic parameter.

Fig. 1 demonstrates the influence of different parameters on the squirt flow effect S. Fig. 1 shows that S item decreases with increasing frequency, illustrating that this local flow squeezes at lower frequency and gets locked at high frequency. Just as Mavko and Jizba (1991) pointed, this kind of squirt flow occurring on local small scale depends heavily on frequency. From Fig. 1(a) we can see that when the crack density is less than a certain value, S varies positively with crack density. But when crack density is greater than a certain value, S decreases. Fig. 1(b) displays the variation of S with respect to the viscosity coefficient. As the viscosity coefficient increases, the total squirt flow effect item S becomes smaller. In other words, squirt flow is a kind of viscous motion within the frequency band of seismic exploration and the squirt effects of water and oil are different because the viscosity of them differs.

Fig. 2(a) displays the real well-log data and Fig. 2(b) gives the comparison of fluid factor f (blue curve) and squirt fluid factor K_{fs} (red curve) on well log, green curve is the result of logging interpretation. Fluid factor is proposed by Russell et al. (2011) and it is expressed as $f = \rho V_p^2 - c\rho V_s^2$ where $c = (V_p/V_s)^2_{dry}$. This factor provides the basis for fluid estimation and acquires favorable effect in practice, but it doesn't consider the local flow effect when porosity and crack coexist. From this figure we can see that, due to the consideration of the effect of fluid flow, K_{fs} appears remarkable anomalous of low values at the existence of fluids and appears high value at the position of dry rock. Through the analysis of this comparison, K_{fs} shows great potential in fluid discrimination.

4. Linearized reflectivity and direct inversion for squirt fluid factor

Amplitude variation with offset (AVO) inversion is a seismic prestack inversion method for estimating fluid and reservoir information. Compared with post-stack seismic inversion, pre-stack seismic inversion allows us to directly estimate various elastic parameters rather than estimating impedance firstly and then calculating elastic parameters indirectly. Russell et al. (2011) derived a generalized AVO approximation by introducing P/S velocity of dry rock to extract fluid, shear modulus and density ($f-m-r$ equation). Eq. (27) is the $f-m-r$ equation proposed by Russell et al. (2011). Using the unified theory proposed by Tang (2011), we re-express the $f-m-r$ equation and formulate a new reflection coefficient approximation with squirt fluid factor K_{fs}.

$$R_{PP}(\theta) = \left[\left(1-\frac{\gamma_{dry}^2}{\gamma_{sat}^2}\right)\frac{\sec^2\theta}{4}\right]\frac{\Delta f}{f} + \left[\frac{\gamma_{dry}^2}{4\gamma_{sat}^2}\sec^2\theta - \frac{2}{\gamma_{sat}^2}\sin^2\theta\right]\frac{\Delta\mu}{\mu} + \left[\frac{1}{2}-\frac{\sec^2\theta}{4}\right]\frac{\Delta\rho}{\rho} \tag{27}$$

Refer to Eqs. (25) and (26),

$$f = \frac{\alpha^2}{\varphi}K_{fs}S \tag{28}$$

The relationship among the fluid factor reflectivity, square of Biot coefficient divided by porosity reflectivity, SFF reflectivity, and total squirt flow effect item reflectivity is,

$$\frac{\Delta f}{f} = \frac{\Delta(\alpha^2/\varphi)}{(\alpha^2/\varphi)} + \frac{\Delta K_{fs}}{K_{fs}} + \frac{\Delta S}{S} \tag{29}$$

Substituting Eq. (29) into Eq. (27) yields,

$$R_{PP}(\theta) = \left[\left(1-\frac{\gamma_{dry}^2}{\gamma_{sat}^2}\right)\frac{\sec^2\theta}{4}\right]\frac{\Delta K_{fs}}{K_{fs}} + \left[\frac{\gamma_{dry}^2}{4\gamma_{sat}^2}\sec^2\theta - \frac{2}{\gamma_{sat}^2}\sin^2\theta\right]\frac{\Delta\mu}{\mu} + \left[\frac{1}{2}-\frac{\sec^2\theta}{4}\right]\frac{\Delta\rho}{\rho} + \left[\left(1-\frac{\gamma_{dry}^2}{\gamma_{sat}^2}\right)\frac{\sec^2\theta}{4}\right]\frac{\Delta(\alpha^2/\varphi/S)}{(\alpha^2/\varphi/S)} + \left(\frac{\sec^2\theta}{2} - \frac{\gamma_{dry}^2}{2\gamma_{sat}^2}\sec^2\theta\right)\frac{\Delta S}{S} \tag{30}$$

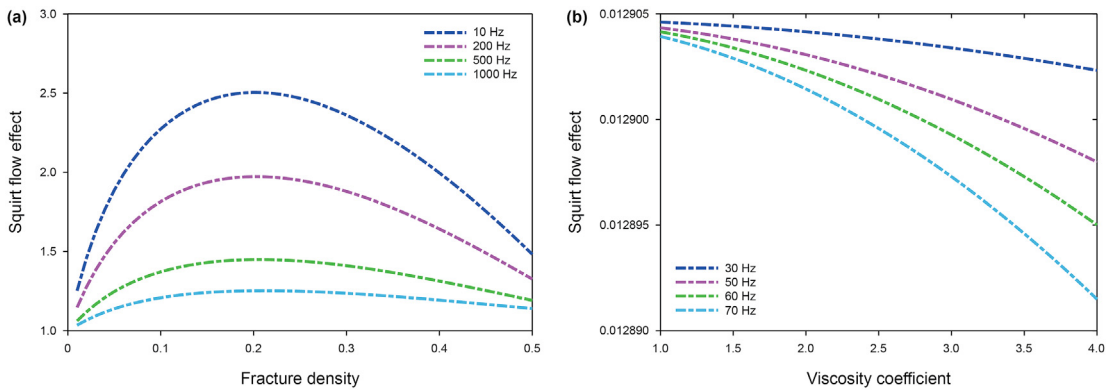

Fig. 1. Analysis of the influence of different parameters on the squirt flow effect. (a) crack density (b) viscosity coefficient.

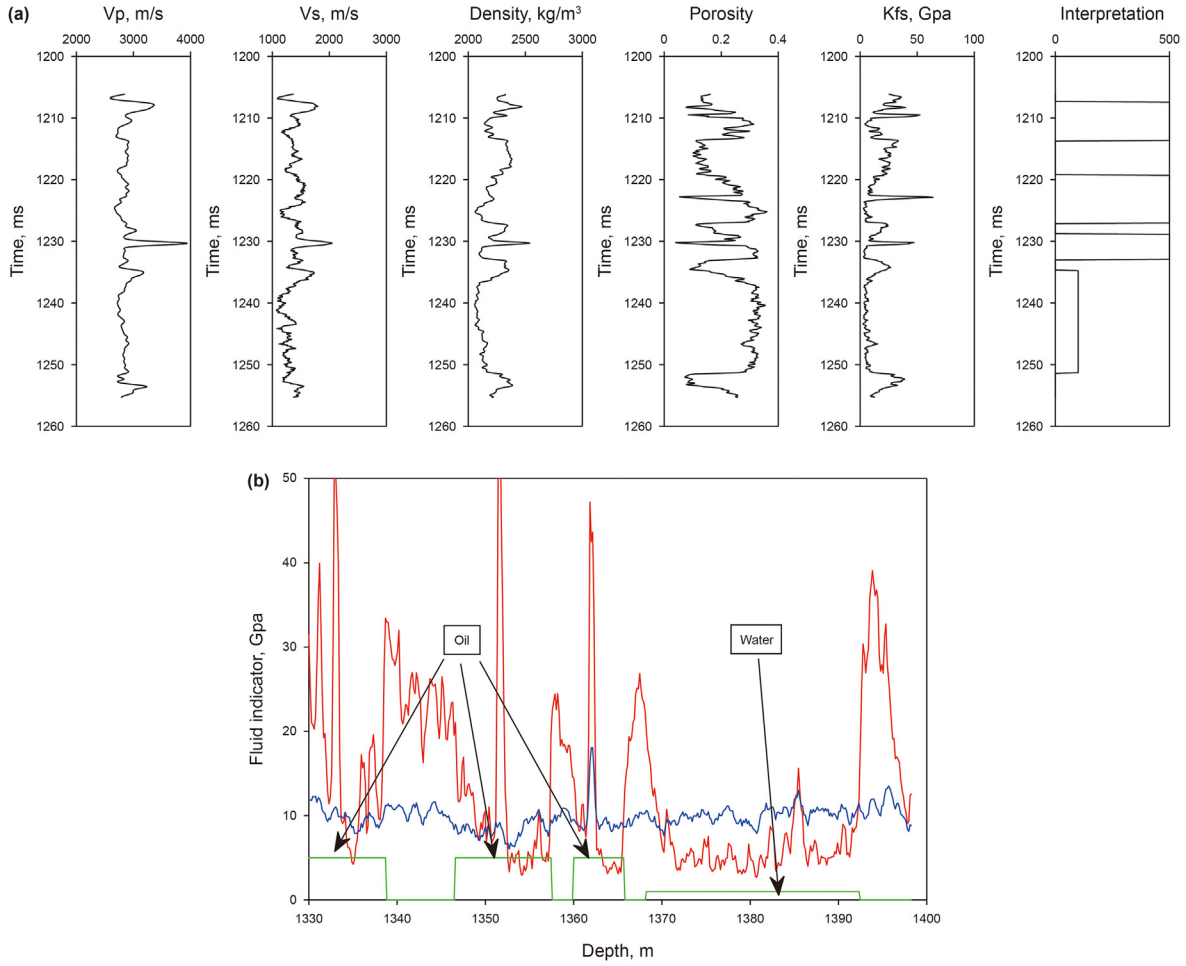

Fig. 2. (a) The real well-log data. (b)The comparison of Russell fluid factor (blue) and squirt fluid factor (red) on well log.

We derive Eq. (30) and get the final reflection coefficient equation in terms of K_{fs},

$$R_{PP}(\theta)=\left[\left(1-\frac{\gamma_{dry}^2}{\gamma_{sat}^2}\right)\frac{\sec^2\theta}{4}\right]\frac{\Delta K_{fs}}{K_{fs}}+\left[\frac{\gamma_{dry}^2}{4\gamma_{sat}^2}\sec^2\theta-\frac{2}{\gamma_{sat}^2}\sin^2\theta\right]\frac{\Delta\mu_s}{\mu_s}+\left[\frac{1}{2}-\frac{\sec^2\theta}{4}\right]\frac{\Delta\rho}{\rho}+\left(\frac{\sec^2\theta}{4}-\frac{2}{\gamma_{sat}^2}\sin^2(\theta)\right)\frac{\Delta(T(\varphi))}{(T(\varphi))}+\left(\frac{\sec^2\theta}{2}-\frac{\gamma_{dry}^2}{2\gamma_{sat}^2}\sec^2\theta\right)\frac{\Delta S}{S} \tag{31}$$

$$\frac{\Delta m}{m}=\frac{2(m_1-m_2)}{(m_1+m_2)} \tag{32}$$

The new reflection coefficient equation contains squirt fluid factor K_{fs}, equivalent shear modulus μ_S, density ρ, gain function $T(\varphi)$ and squirt flow effect S.

where $S=1+S(\omega)N$, $\mu_S=\frac{\mu}{T(\varphi)}$, $T(\varphi)=\alpha^2\varphi^{-1}S^{-1}$, $\gamma_{dry}=(V_p/V_s)_{dry}$, and $\gamma_{sat}=(V_p/V_s)_{sat}$.

θ is incident angle, m_1 represents the elastic parameters upper the reflection interface and m_2 represents the parameters below the reflection interface, respectively. By introducing total squirt flow effect item into the equation, we can estimate the fluid modulus in the coexistence of pores and cracks. And we can take two important parameters of crack into consideration, crack density and crack aspect ratio. This new reflection coefficient equation is derived with the following assumptions including plane waves, small incident angle range and small relative changes in elastic parameters occur across the boundary.

To verify the accuracy of Eq. (31), we set three models containing P-velocity V_p, S-velocity V_s, density ρ, porosity φ, crack density ε and crack aspect ratio γ as shown in Table 1. Model 1 is a dry reflector. The porosity of each layer is equally 16% and the upper P-impedance is smaller than the lower layer. Model 2 is a dry-water reflector. The upper layer is dry sand layer and the porosity is 16% while the lower layer is water sand and the porosity is 18%. Model 3 is water-gas reflector. The pore fluid is different and porosity are different. In these three models, we set the crack density as 0.15 in dry sand and 0.2 in fluid sand to calculate the squirt fluid factor K_{fs}. Fig. 3 shows the comparison of different reflection coefficient curves. Curves in blue, black and red denote the reflection coefficients calculated from the exact Zoeppritz equation, Aki-Richards approximate equation and Eq. (31) respectively. Fig. 3(a) displays the comparison of reflection coefficient curves calculated by exact Zoeppritz equation (blue curve), Aki-Richards approximate equation (black curve) and proposed equation (red curve) of model 1. Fig. 3(c) displays the comparison of reflection coefficient curves respectively calculated by exact Zoeppritz equation (blue curve), Aki-Richards approximate equation (black curve) and proposed equation (red curve) of model 2. Fig. 3(e) displays the comparison of reflection coefficient curves calculated by exact

Zoeppritz equation (blue curve), Aki-Richards approximate equation (black curve) and proposed equation (red curve) of model 3. Fig. 3(b, d, f) show the difference between reflection coefficients from the exact Zoeppritz equation and Eq. (31) of three models, respectively. In model 1, the AVO curve calculated by Eq. (31) is very close to the AVO curve calculated by the Zoeppritz equation and the Aki-Richards approximation. Because the derivation of Eq. (31) begins with the Aki-Richards approximation, the two equations give similar AVO curves in dry reflector. In model 2, AVO curves calculated by Aki-Richards approximation and Eq. (31) are almost the same, and both curves are close to Zoeppritz curve when the incidence angle is less than 30°. However, as the incidence angle increases, the AVO curves calculated by the Aki-Richards approximation and Eq. (31) deviates from those by Zoeppritz equation. Because the density of the upper and lower layers is different due to the change of porosity, besides, the effect of porosity on velocity is greater than that of pore fluid. Thus, at large incident angles, porosity differences lead to large variations in P-wave and S-wave velocities, resulting in large errors between the AVO approximation and the precise Zoeppritz equation. In model 3, we note that the AVO curves calculated by Eq. (31) and the Aki-Richards approximation are almost identical, and both are very close to those by Zoeppritz equation in the range of incident angles less than 30°. However, when the incident angle is large, the two curves do not fit with Zoeppritz curve. This is because the change of fluid content and porosity leads to the larger change of P-velocity and S-velocity, which makes the AVO approximation less effective at large incident angle. To summarize, from these figures we can see that although the red curve is not exactly identical with two others, they are very close, especially when the incident angle is less than 30°. Therefore, the new reflection coefficient is reasonably feasible and accurate. And because the incident angle of practical seismic exploration is usually less than 40°, we can conclude that the new reflection coefficient equation can be utilized to invert the fluid factor stably in practical applications.

To find out whether the elastic parameters can be well estimated from pre-stack seismic data, we analyze the contribution of each parameters to the reflection coefficient. Fig. 4 shows the reflection coefficient of Eq. (31) in terms of five parameters such as squirt fluid factor K_{fs}, equivalent shear modulus μ_s, density ρ, etc. The red curve is the reflection coefficient calculated with the parameters in model 1. Fig. 4(a) shows the reflection coefficient varied with the squirt fluid factor K_{fs}. From this figure we can see that when K_{fs} varies from 80% to 120%, the reflection coefficient shows apparent change. Thus, we can assume that K_{fs} is a main contributor to Eq. (31), which means that the estimation of K_{fs} from seismic data is possible. From Fig. 4(b) and (e) we can see that, the contributions of μ_s and ρ to reflection coefficient are very similar and both of the reflection coefficients decrease as the incident angle increases. This phenomenon indicates the great correlation of μ_s and ρ, so it is difficult for us to extract density from seismic data. However, to get a reliable inversion result only the large contribution is inadequate, such as $T(\varphi)$ in Fig. 4(c). $T(\varphi)$ is a gain function without no geophysical meaning, being a couple term of squirt flow effect S, porosity φ and Biot coefficient α. Fig. 4(d) shows the reflection coefficient varied with the squirt flow effect S. We can see that although S is a useful parameter for us to describe the subsurface fluid, the contribution of it to reflection coefficient is small.

Furthermore, we apply AVO inversion based on Bayesian framework and incorporate Eq. (31) and seismic wavelet as forward solver to directly estimate the elastic parameters. The constraint of smooth model in objective function is conducive to a more stable result. With the Bayesian inversion theory, we assume that prior distribution obeys the Cauchy distribution. Cauchy distribution is a long-tail probability distribution which can improve the resolution of inversion result. And we assume the likelihood function obeys the Gaussian distribution to obtain the posterior probability density function. Finally, we utilize a method of iteratively reweighted least square to solve the objective function.

With Eq. (31) and convolution model as forward solver, we estimate squirt fluid factor K_{fs} in Bayesian frame.

Defining $\Delta \ln m = \frac{\Delta m}{m}$, Eq. (31) changes to,

$$R_{PP}(\theta) = a(\theta)\Delta \ln K_{fs} + b(\theta)\Delta \ln \mu_s + c(\theta)\Delta \ln \rho + d(\theta)\Delta \ln S + e(\theta)\Delta \ln T(\varphi) \tag{33}$$

where

$$a(\theta) = \left[\left(1 - \frac{\gamma_{dry}^2}{\gamma_{sat}^2}\right)\frac{\sec^2\theta}{4}\right]$$

$$b(\theta) = \left[\frac{\gamma_{dry}^2}{4\gamma_{sat}^2}\sec^2\theta - \frac{2}{\gamma_{sat}^2}\sin^2\theta\right]$$

$$c(\theta) = \left[\frac{1}{2} - \frac{\sec^2\theta}{4}\right]$$

$$d(\theta) = \left(\frac{\sec^2\theta}{4} - \frac{2}{\gamma_{sat}^2}\sin^2(\theta)\right)$$

$$e(\theta) = \left(\frac{\sec^2\theta}{2} - \frac{\gamma_{dry}^2}{2\gamma_{sat}^2}\sec^2\theta\right)$$

$$\mathbf{R} = [R_1\ R_2\ R_3\ R_4\ R_5] = \left[\Delta \ln K_{fs}\ \Delta \ln \mu_s\ \Delta \ln \rho\ \Delta \ln T(\varphi)\ \Delta \ln S\right] \tag{34}$$

$$\mathbf{M} = [a(\theta)\ b(\theta)\ c(\theta)\ d(\theta)\ e(\theta)] \tag{35}$$

We assume the parameters to be estimated obey Cauchy prior distribution and the likelihood function obeys Gaussian probability density distribution. The posterior probability function is stated as,

$$p(\mathbf{R},|\mathbf{D}) \propto \prod_{i=1}^{n}\left[\frac{1}{1 + R_i^2/\sigma_m^2}\right]\cdot\exp\left[\frac{-(\mathbf{D}-\mathbf{WMR})^T(\mathbf{D}-\mathbf{WMR})}{2\sigma_n^2}\right] \tag{36}$$

where $\mathbf{R}$ is the corresponding reflectivity of SFF, equivalent shear modulus, density, gain function and total squirt flow effect item, $\mathbf{D}$ is observed seismic record, $\mathbf{W}$ is wavelet matrix, n is the number of sampling points per trace, σ_m^2 is the model parameters variance and σ_n^2 is noise variance of seismic data.

The objective function is,

Table 1
Values of parameters for water-bearing and gas-bearing model.

		V_p, m/s	V_s, m/s	ρ, kg/m^3	φ	ε	γ
Model 1	Dry sand	3680	1685	2565	16%	0.15	0.001
	Dry sand	3685	1670	2600	16%	0.15	0.001
Model 2	Dry sand	3530	1820	2570	16%	0.15	0.001
	Water sand	3628	1880	2420	18%	0.2	0.001
Model 3	Water sand	3660	2050	2450	23%	0.2	0.001
	Gas sand	3680	2100	2435	23%	0.2	0.001

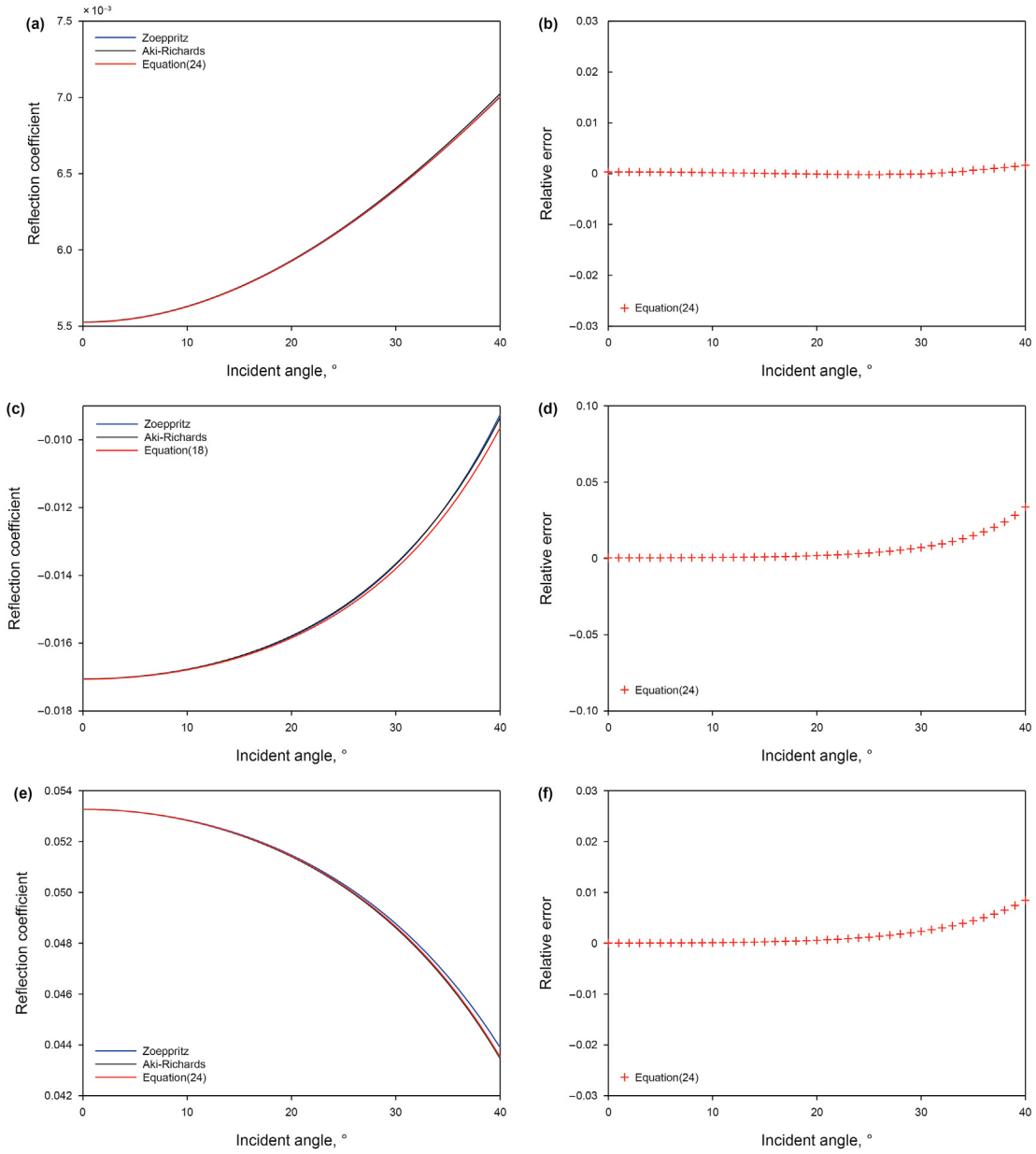

Fig. 3. Comparison of different reflection coefficient curves. Curves in blue, black and red denotes the reflection coefficients calculated from the exact Zoeppritz equation, Aki-Richards approximate equation and Eq. (31) respectively. (a) Comparison of reflection coefficient curves of model 1. (b) Difference between reflection coefficients from the exact Zoeppritz equation and Eq. (31) of model 1. (c) Comparison of reflection coefficient curves of model 2. (d) Difference between reflection coefficients from the exact Zoeppritz equation and Eq. (31) of model 2 (e) Comparison of reflection coefficient curves of model 3. (f) Difference between reflection coefficients from the exact Zoeppritz equation and Eq. (31) of model 3.

$$F_{\mathrm{OB}} = (\mathbf{D} - \mathbf{WMR})^{\mathrm{T}}(\mathbf{D} - \mathbf{WMR}) + 2\sigma_{\mathrm{n}}^2 \sum_{i=1}^{n} \ln\left(1 + R_i^2 \Big/ \sigma_{\mathrm{m}}^2\right) + \Lambda \tag{37}$$

Λ is the model constraint,

$$\Lambda = \sum_{i=1}^{5} \lambda_i (\eta_i - qR_i)^{\mathrm{T}} (\eta_i - qR_i) \tag{38}$$

where $0 < \lambda_i < 1$ is constraint coefficient for elastic parameters to be solved $\eta_i = \frac{1}{2}\ln\left(\frac{m_i}{m_{i0}}\right)$, m_i is different elastic parameters, m_{i0} is the initial value of per trace, $q = \int_{t_0}^{t} \mathrm{d}\tau$.

Finally, we use the method of iteratively reweighted least square to optimize and solve the objective equation (Yin et al., 2016; Zong et al., 2018; Ma et al., 2019).

To test the feasibility and practicability of our proposed pre-stack inversion method, we use a series data modified from well log in an oil field as model parameters. The P-velocity, S-velocity, density and porosity are taken from the well logging data. And squirt fluid factor is calculated from the well log based on the petrophysical theory. Synthetic angle gathers are generated by convolving the model reflection coefficients and 30 Hz Ricker wavelet with exact Zoeppritz equation. Fig. 5 shows the synthetic

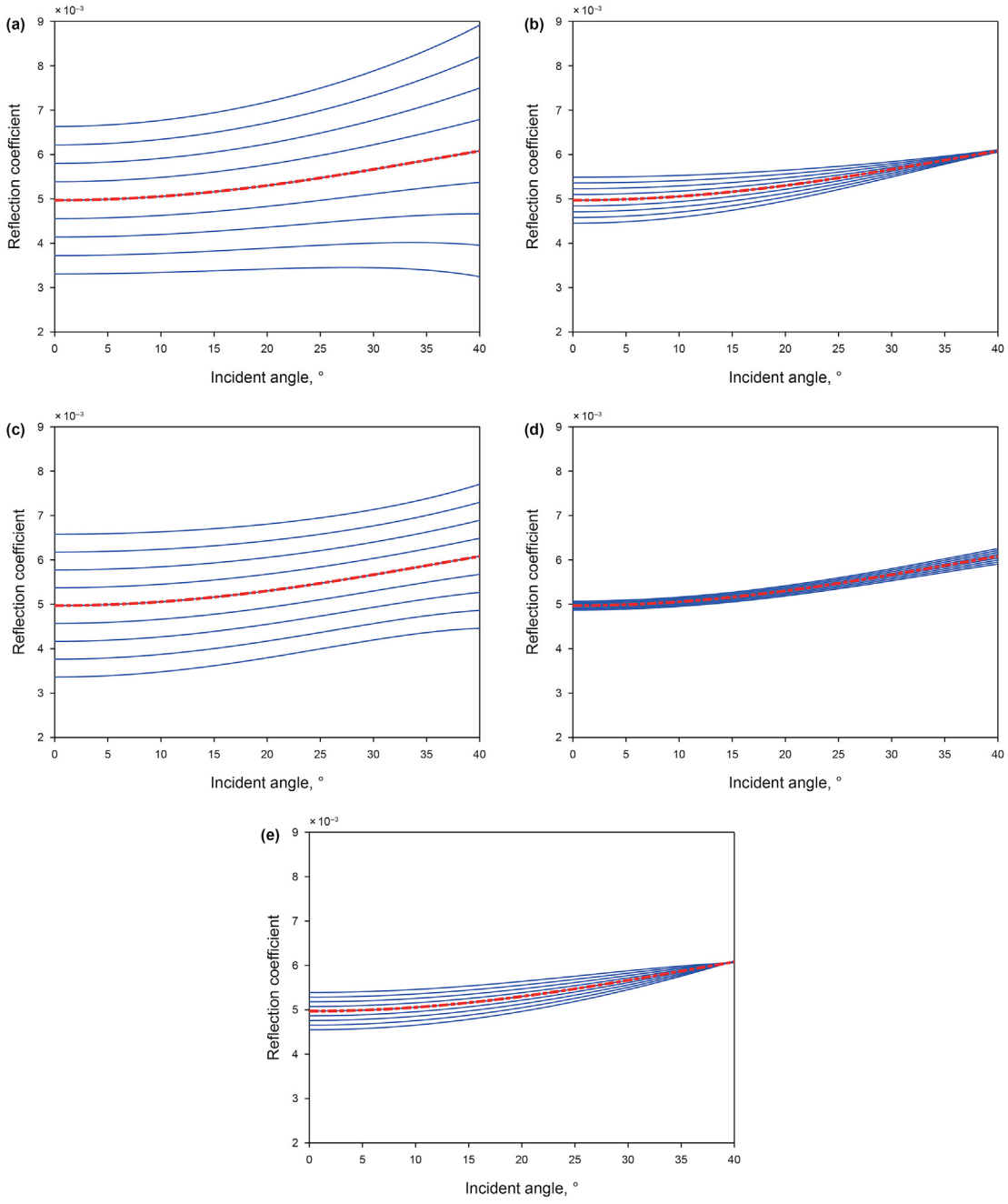

Fig. 4. Elastic parameters contribution analysis of Eq. (31). Red curve is the reflection coefficient calculated in model 1. Blue curves are reflection coefficient of different parameters varied from 80% to 120%. (a) Reflection coefficient varied with the squirt fluid factor K_{fs}. (b) Reflection coefficient varied with the equivalent shear modulus μ_s. (c) Reflection coefficient varied with the gain function $T(\varphi)$. (d) Reflection coefficient varied with the total squirt flow effect item S. (e) Reflection coefficient varied with the density (ρ).

angle gather data with different signal to noise ratios (S/N). The time window is from 2000 ms to 2800 ms, and the incident angle range is 0°–30° and time sampling interval is 2 ms. Fig. 5(a) is the synthetic seismogram profile with no noise. Fig. 5(b) is the synthetic seismogram profile with S/N equal to 5. Fig. 5(c) is the synthetic seismogram profile with S/N equal to 2.

Fig. 6 displays the estimated model parameters from synthetic data. The original squirt fluid factor K_{fs}, equivalent fluid modulus μ_s, gain function $T(\varphi)$, squirt flow effect S and density ρ are displayed in black curves. Red curve displays the inversion result and green curve displays the smooth initial model. From Fig. 6(a), the inversion result of each parameter fits well with the original model parameter in the situation of no noise. When the S/N equals to 5, we still can obtain stable inversion results of K_{fs} and S as Fig. 6(b) shows. However, the inversion result of density appeared remarkable deviation. It is known that density is difficult to invert accurately, and there are two primary reasons (Kabir et al., 2006). Firstly the contribution of density to reflectivity is small. Secondly the correlation between density and other parameters is strong (Zong et al., 2017). Fig. 6(c) shows the inversion results in the situation of S/N is 2. The error between inverted result of K_{fs} and real value is moderate so it's a stable parameter to discriminate fluid. What's

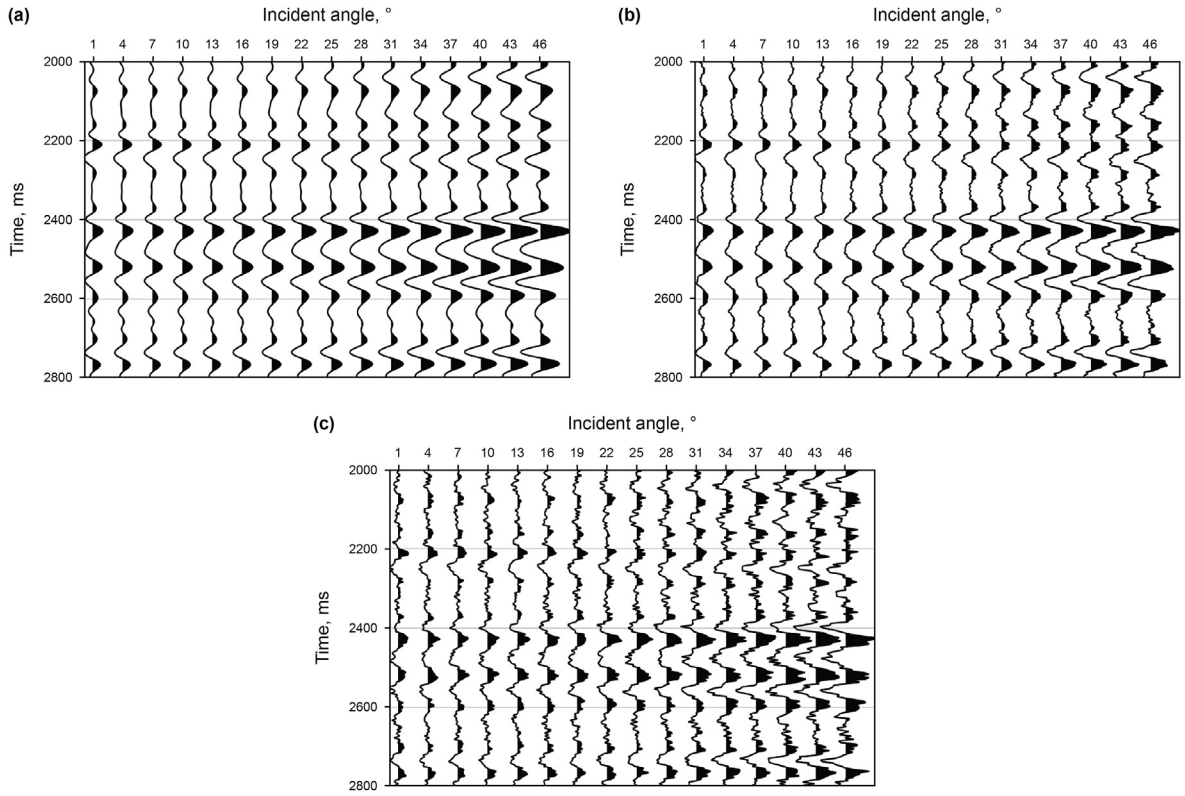

Fig. 5. Synthetic angle gather data with different S/N. (a) No noise. (b) S/N = 5 (c) S/N = 2.

more, S indicates the squirt effect of pore fluid and it also can be estimated from angle gather data.

5. Field data application

We utilize an actual example to investigate the robustness of the proposed pre-stack seismic inversion method, a suite of seismic data from a gulf are used in this section. The survey line passes through two wells (well A and well B). Two reservoirs in well A are both water bearing. The upper formation is cracked but the lower formation is not cracked. Two reservoirs in well A are oil bearing. Seismic data are obtained from the measurements of dual sensor (velocity geophone and pressure geophone) and is processed by the contractor to ensure that the final prestack amplitude imaging underground interface reflection strength should be correct as much as possible. The converted wave, anisotropy effects, and interbed multiples are ignored after processing. Besides, the seismic data has been treated with fidelity processing and amplitude preserved processing (Li et al., 2017; Vitale et al., 2018). The maximum incident angle is around 30° and we perform the partial angle-stack processing with five incident angle ranges, 0°–6°, 6°–12°, 12°–18°, 18°–24°, 24°–30°. Five partial angle-stack seismic profiles are shown in Fig. 7. Fig. 7(a) is partial angle-stack seismic profile with incident angle 0°–6°, Fig. 7(b) is partial angle-stack seismic profile with incident angle 6°–12°, Fig. 7(c) is partial angle-stack seismic profile with incident angle 12°–18°, Fig. 7(d) is partial angle-stack seismic profile with incident angle 18°–24°, Fig. 7(e) is partial angle-stack seismic profile with incident angle 24°–30°. The time window of seismic data is from 1900 ms to 2200 ms and time sampling interval is 2 ms. The frequency band varies from 5 to 70 Hz, and the main frequency is 27 Hz.

Well A is used in the process of seismic inversion or initial model construction. Two oil bearing reservoirs in well A are near 1970 ms and 2050 ms (the position marked red); the blue position indicates the existence of water sand and white is other thing else. Fig. 8 shows the estimated parameters of field with the proposed method. Fig. 8(a-c) display squirt fluid factor K_{fs}, squirt flow effect term S and density ρ, respectively. From the figure we can see that, for the overlying oil sand and underlying oil sand, squirt fluid factor appears anomalously low value and squirt flow effect term shows anomalously high value. Besides, density shows low value anomaly at oil sand. In general, the inversion results make the difference between oil layer and dry layer more obvious and show good correlation with the fluid interpretation. The squirt flow effect of medium with fluid filled pores and cracks is very intuitive when the external force acts. And S can effectively reflect this phenomenon under the elastic wave action as Fig. 8(b) shows. Squirt fluid factor K_{fs} is equal to fluid modulus K_f divided by S, so K_{fs} shows the lower anomaly when the squirt flow occurs. According to the field data example, the proposed squirt fluid factor shows the effectiveness in fluid discrimination. To ensure the stability of the inversion, firstly, we processed the field seismic data to ensure the quality of seismic data. Furthermore, the parameter to be inverted is a main contributor to reflection coefficient equation by the contribution analysis. Finally, prestack seismic inversion utilized the model constraints and iteratively reweighted least square method to optimize and solve the equation.

To test the feasibility of the proposed inversion approach in field data, we use well B to verify the effectiveness of proposed method in field data example. Two water bearing reservoirs in well B are near 1020 ms and 1055 ms (the position marked blue). Fig. 9(a) and (b) are the estimation of Russell fluid factor and P-impedance of field data, respectively. From Fig. 9(a) we can see that the Russell fluid factor inversion result shows low value anomaly at both water

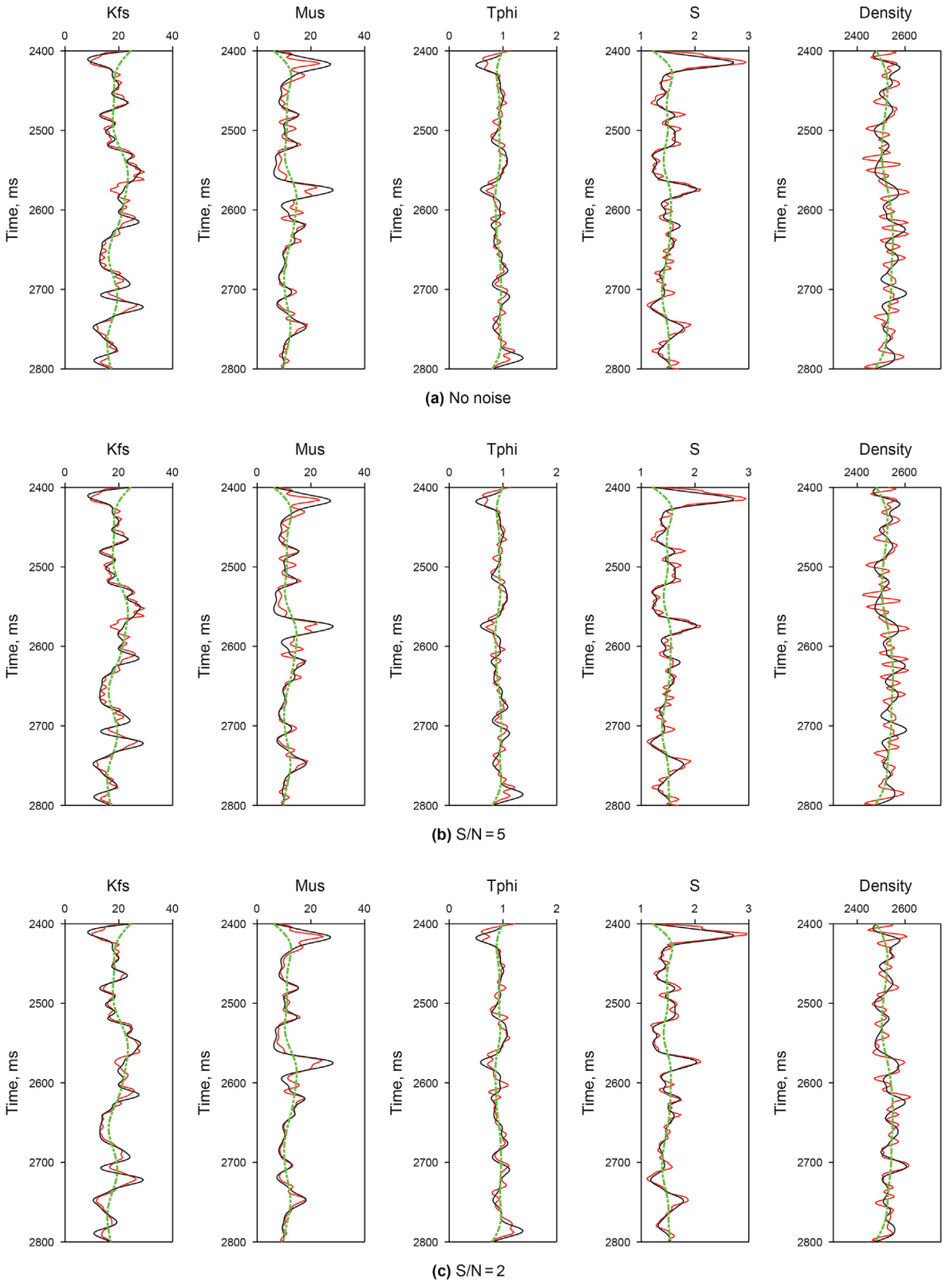

Fig. 6. Inversion results of elastic parameters from synthetic data. Red line is inversion result, black line is model data, and green line is smooth initial model. (a) No noise. (b) S/N = 5. (c) S/N = 2.

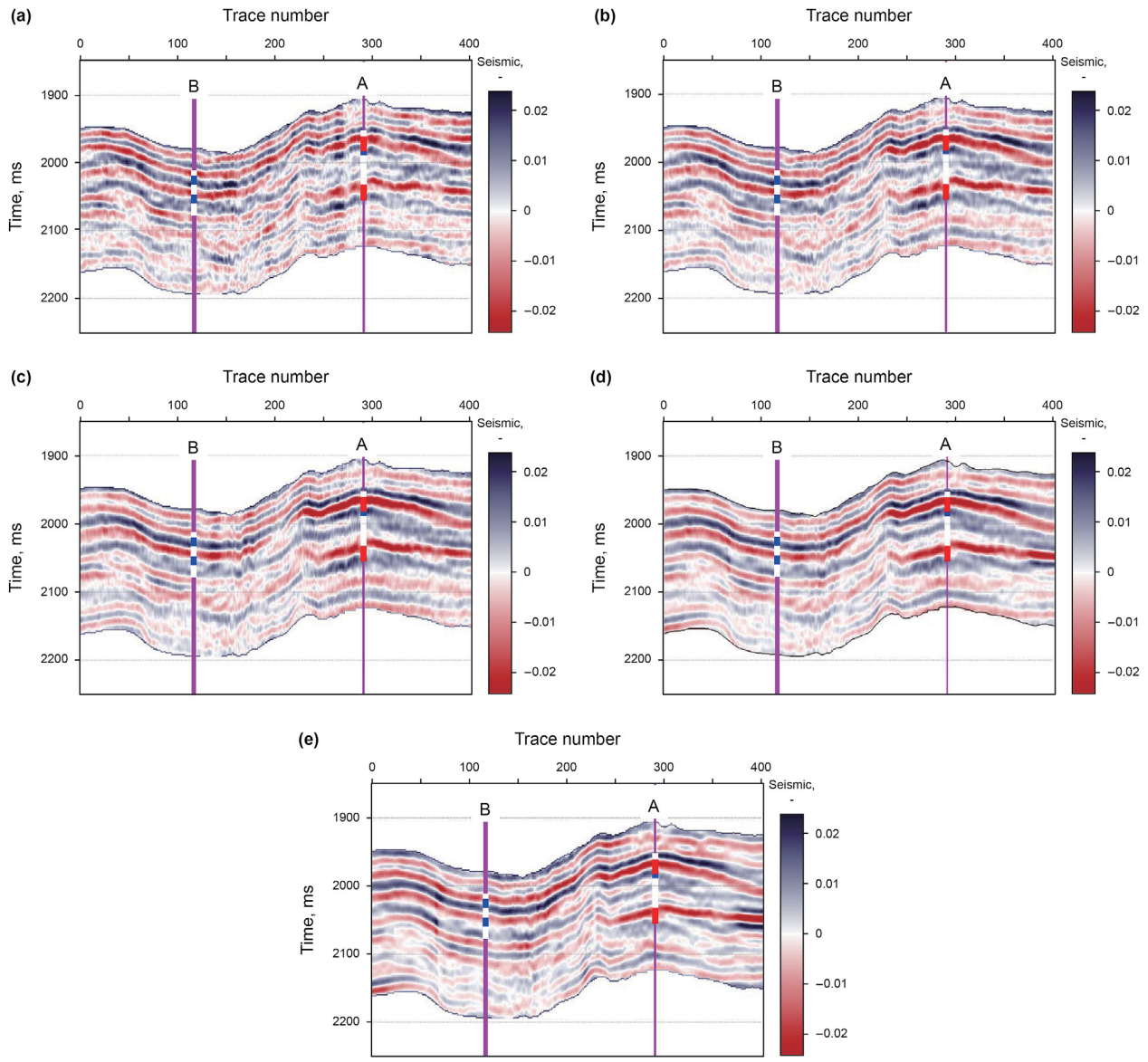

Fig. 7. Partial angle-stack seismic profiles with different incident angle ranges. (a) Partial angle-stack seismic profile with incident angle 0°–6°. (b) Partial angle-stack seismic profile with incident angle 6°–12°. (c) Partial angle-stack seismic profile with incident angle 12°–18°. (d) Partial angle-stack seismic profile with incident angle 18°–24°. (e) Partial angle-stack seismic profile with incident angle 24°–30°.

bearing reservoirs and oil bearing reservoirs, which makes ambiguous fluid discrimination results. In Fig. 9(b) we can see that P-impedance shows low value anomaly at upper water reservoir but no obvious anomaly at lower water reservoir. Because the upper reservoir contains cracks, while the lower reservoir does not. The existence of crack in reservoir leads to low value anomaly of P-impedance. However, the P-impedance itself is insensitive to the fluid, which causes less significantly lower anomaly. In contrast, the squirt flow can make the difference between water bearing reservoir and oil bearing reservoir more obvious by considering the squirt flow effect between cracks and pores. Therefore, according to the contrasts of different inverted fluid factors, the squirt fluid factor is more reliable and feasible to discriminate fluid.

6. Discussion

Russell fluid factor is constructed based on Biot theory, this theory doesn't consider the cracks but only take pores into consideration. And assumption of uniform distribution of pores ignores the influence of squirt flow on wave propagation. In order to more accurately describe reservoir fluid in case of pores and cracks coexist, we build a squirt fluid factor based on Tang's cracked porous medium elastic wave theory. By testing with model parameters, seismic data and well data, we demonstrate that the squirt fluid factor can predict the presence of possible hydrocarbon sand and reduce the illusion of fluid identification.

However, this study has several limitations. First, there are up to five parameters in the AVO inversion so that the prediction accuracy and stability is still need to be improved. To solve this problem, we can try to develop more stable inversion algorithm or calculate more reasonable low-frequency initial model in AVO inversion by broadband inversion method, etc. (Zong et al., 2018). Second, how to reveal the multi-frequency information in fluid factor as much as possible remains challenging in the future study. In a word, the

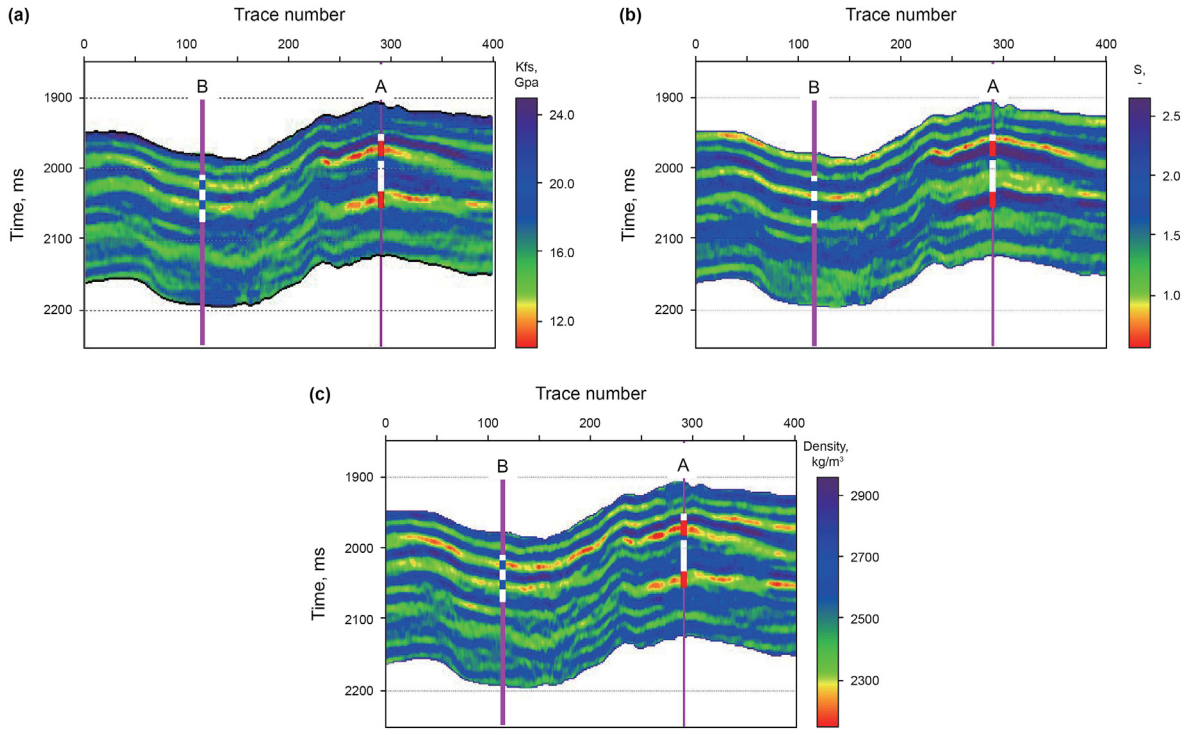

Fig. 8. Estimation of parameters of field data with the proposed method. (a) Squirt fluid factor. (b) Squirt flow effect term. (c) Density. Red position on well A is oil and blue position on well A is water.

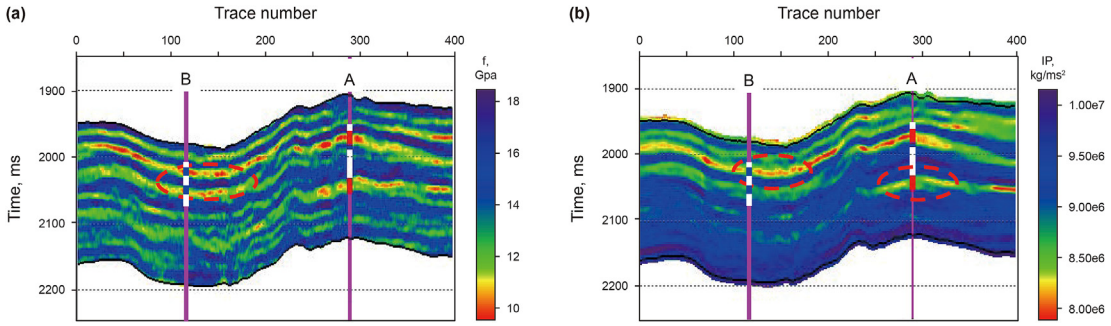

Fig. 9. Estimation of parameters of field data. (a) P-impedance. (b) Russell fluid factor.

prime objective of this paper is to estimate the squirt fluid factor from prestack seismic data and we think that the goal is achieved. We construct a squirt fluid factor based on the cracked porous medium elastic wave theory, which can lead to more reliable fluid discrimination result in seismic exploration.

7. Conclusion

Combining the unified theory for elastic wave propagation through porous media containing cracks and petrophysical theory, we develop a novel AVO pre-stack seismic inversion method for fluid discrimination. A novel fluid indicator considering squirt flow effect is constructed. Based on the squirt fluid factor, we derive a new reflection coefficient equation. The precision analysis confirms the effectiveness of the reflection coefficient equation. The elastic parameters contribution analysis of reflection coefficient equation demonstrates that the squirt fluid factor can be effectively extracted from the seismic data. The consideration of squirt flow effect in the proposed method can diminish the ambiguity of fluid discrimination and the Bayesian frame improves the stability of inversion method. The model test verifies the feasibility and field data example illustrates the practicability of this AVO inversion approach.

Acknowledgements

We would like to acknowledge the sponsorship of National Natural Science Foundation of China (41974119, 42030103) and Science Foundation from Innovation and Technology Support Program for Young Scientists in Colleges of Shandong Province and Ministry of Science and Technology of China (2019RA2136) and Marine S&T Fund of Shandong Province for Pilot National Laboratory for Marine Science and Technology (Qingdao) (2021QNLM020001-6).

References

Allen, J.L., Peddy, C.P., Fasnacht, T.L., 1993. Some AVO failures and what (we think) we have learned. Lead. Edge 12 (3), 162.

Barak, M.S., Kumari, M., Kumar, M., 2018. Effect of local fluid flow on the propagation of plane waves at an interface of water/double-porosity solid with underlying uniform elastic solid. Ocean. Eng. 147, 195–205. https://doi.org/10.1016/j.oceaneng.2017.10.030.
Batzle, M.L., 2004. Gassmann's equation and fluid-saturation effects on seismic velocities. Geophysics 69 (2), 398–405.
Batzle, M.L., Han, D.H., Castagna, J.P., 1995. Fluid effects on bright spot and AVO analysis. SEG Technical Program Expanded Abstracts 1995: Society of Exploration Geophysicists 1119–1121.
Biot, M.A., 1956a. Theory of elastic waves in a fluid-saturated porous solid. 1. Low frequency range. J. Acoust. Soc. Am. 28, 168–178. https://doi.org/10.1121/1.1908239.
Biot, M.A., 1956b. Theory of propagation of elastic waves in a fluid-saturated porous solid. II. Higher frequency range. J. Acoust. Soc. Am. 28 (2), 179–191. https://doi.org/10.1121/1.1908241.
Cichostępski, K., Kwietniak, A., Dec, J., 2019. Verification of bright spots in the presence of thin beds by AVO and spectral analysis in Miocene sediments of Carpathian Foredeep. Acta Geophys. 67 (6), 1731–1745. https://doi.org/10.1007/s11600-019-00324-z.
Dashti, M., Stuart, A.M., 2016. The bayesian approach to inverse problems. In: Ghanem, Roger, David Higdon, Owhadi, Houman (Eds.), Handbook of Uncertainty Quantification. Springer International Publishing, pp. 1–118.
Downton, J., 2005. Seismic Parameter Estimation from AVO Inversion.
Downton, J.E., Ursenbach, C., 2006. Linearized amplitude variation with offset (AVO) inversion with supercritical angles. Geophysics 71 (5), E49–E55. https://doi.org/10.1190/1.2227617.
Gholami, A., Aghamiry, H.S., Abbasi, M., 2018. Constrained nonlinear amplitude variation with offset inversion using Zoeppritz equations. Geophysics 83 (3), R245–R255. https://doi.org/10.1190/geo2017-0543.1.
Goodway, W., Chen, T., Downton, J., 1997. Improved AVO fluid detection and lithology discrimination using Lamé parameters; lr, mr and 1/m fluid stack from P and S inversions. In: CSEG National Convention Expanded Abstracts.
Kabir, N., Crider, R., Ramkhelawan, R., Baynes, C., 2006. Can hydrocarbon saturation be estimated using density contrast parameter? CSEG Recorder CX31–CX37.
Kumar, M., Kumari, M., Barak, M.S., 2018. Reflection of plane seismic waves at the surface of double-porosity dual-permeability materials. Petrol. Sci. 15 (3), 521–537. https://doi.org/10.1007/s12182-018-0245-y.
Kumar, M., Kumari, M., 2020. Horizontal and vertical motion at the surface of swelling poroelastic layer sandwiched between water and elastic solid. Ocean. Eng. 210, 107551. https://doi.org/10.1016/j.oceaneng.2020.107551.
Kumar, M., Barak, M.S., Kumari, M., 2019. Reflection and refraction of plane waves at the boundary of an elastic solid and double-porosity dual-permeability materials. Petrol. Sci. https://doi.org/10.1007/s12182-018-0289-z.
Kumari, M., Kumar, M., 2020. Reflection of Inhomogeneous Waves at the Surface of a Cracked Porous Solid with Penny-Shaped Inclusions: Waves in Random and Complex Media, pp. 1–22. https://doi.org/10.1080/17455030.2020.1842555.
Kumari, M., Kumar, M., Barak, M.S., 2021. Wave propagation characteristics at the welded interface of double-porosity solid and double-porosity dual-permeability materials. Waves Random Complex Media 31 (6), 1682–1707. https://doi.org/10.1080/17455030.2019.1698789.
Kumari, M., Barak, M.S., Kumar, M., 2017. Seismic reflection and transmission coefficients of a single layer sandwiched between two dissimilar poroelastic solids. Petrol. Sci. 14 (4), 676–693. https://doi.org/10.1007/s12182-017-0195-9.
Li, H., Zhang, J., Cai, S., Pan, H., 2020a. A two-step method to apply Xu–Payne multi-porosity model to estimate pore type from seismic data for carbonate reservoirs. Petrol. Sci. 17 (3), 615–627. https://doi.org/10.1007/s12182-020-00440-2.
Lang, X., Grana, D., 2018. Bayesian linearized petrophysical AVO inversion. Geophysics 83 (3), M1–M13. https://doi.org/10.1190/geo2017-0364.1.
Li, K., Yin, X., Zong, Z., 2017. Pre-stack Bayesian cascade AVA inversion in complex-Laplace domain and its application to the broadband data acquired at East China. J. Petrol. Sci. Eng. 158, 751–765. https://doi.org/10.1016/j.petrol.2017.09.005.
Li, K., Yin, X., Zong, Z., Lin, H., 2020b. Seismic AVO statistical inversion incorporating poroelasticity. Petrol. Sci. 17 (5), 1237–1258. https://doi.org/10.1007/s12182-020-00483-5.
Liu, C., Ghosh, D., 2017. A new seismic attribute for ambiguity reduction in hydrocarbon prediction. Geophys. Prospect. 65 (1), 229–239. https://doi.org/10.1111/1365-2478.12367.
Ma, Z., Yin, X., Zong, Z., et al., 2019. Azimuthally variation of elastic impedances for fracture estimation. J. Petrol. Sci. Eng. 181, 106112. https://doi.org/10.1016/j.petrol.2019.05.063.
Mavko, G., Jizba, D., 1991. Estimating grain-scale fluid effects on velocity dispersion in rocks. Geophysics 56 (12), 1940–1949. https://doi.org/10.1190/1.1443005.
Mavko, G., Nur, A., 1975. Melt squirt in the asthenosphere. J. Geophys. Res. 80 (11), 1444–1448. https://doi.org/10.1029/JB080i011p01444.
Mazzotti, A., 1990. Prestack amplitude analysis methodology and application to seismic bright spots in the Po Valley. Geophysics 55 (2), 157–166. https://doi.org/10.1190/1.1442822.
Mollajan, A., Memarian, H., Quintal, B., 2019. Imperialist competitive algorithm optimization method for nonlinear amplitude variation with angle inversion. Geophysics 84 (3), N81–N92. https://doi.org/10.1190/geo2018-0507.1.
Murphy, W.F., Winkler, K.W., Kleinberg, R.L., 1986. Acoustic relaxation in sedimentary rocks: dependence on grain contacts and fluid saturation. Geophysics 51 (3), 757–766. https://doi.org/10.1190/1.1442128.
Myśliwiec, M., 2004. Poszukiwania złóż gazu ziemnego w osadach miocenu zapadliska przedkarpackiego na podstawie interpretacji anomalii sejsmicznych—podstawy fizyczne i dotychczasowe wyniki. Przeglad Geol. 52, 299–306.
O'Connell, R.J., Budiansky, B., 1977. Viscoelastic properties of fluid-saturated cracked solids. J. Geophys. Res. 82 (36), 5719–5735. https://doi.org/10.1029/JB082i036p05719.
Ross, C.P., Kinman, D.L., 1995. Nonbright-spot AVO: two examples. Geophysics 60 (5), 1398–1408. https://doi.org/10.1190/1.1443875.
Russell, B., Gray, D., Hampson, D., 2011. Linearized AVO and poroelasticity. Geophysics 76 (3), C19–C29. https://doi.org/10.1190/1.3555082.
Russell, B.H., Hedlin, K., Hilterman, F.J., et al., 2003. Fluid-property discrimination with AVO: a Biot-Gassmann perspective. Geophysics 68 (1), 29–39.
Shaw, R.K., Sen, M.K., 2006. Use of AVOA data to estimate fluid indicator in a vertically fractured medium. Geophysics 71 (3), C15–C24. https://doi.org/10.1190/1.2194896.
Shuey, R.T., 1985. A simplification of the Zoeppritz equations. Geophysics 50 (4), 609–614. https://doi.org/10.1190/1.1441936.
Skopintseva, L., Ayzenberg, M., Landrø, M., et al., 2011. Long-offset AVO inversion of PP reflections from plane interfaces using effective reflection coefficients. Geophysics 76 (6), C65–C79. https://doi.org/10.1190/geo2010-0079.1.
Smith, G.C., Gidlow, P.M., 1987. Weighted stacking for rock property estimation and detection OF gas. Geophys. Prospect. 35 (9), 993–1014. https://doi.org/10.1111/j.1365-2478.1987.tb00856.x.
Tor, E.R., Håkon, T., Bjørn, U., 2008. Nonlinear Bayesian joint inversion of seismic reflection coefficients. Geophys. J. Int. 173 (1), 265–280.
Tang, X., 2011. A Unified Theory for Elastic Wave Propagation through Porous Media Containing Cracks—An Extension of Biot's Poroelastic Wave Theory: China Earth, pp. 784–795.
Tang, X., Chen, X., Xu, X., 2012. A cracked porous medium elastic wave theory and its application to interpreting acoustic data from tight formations. Geophysics 77 (6), D245–D252.
Thomsen, L., 1985. Biot-consistent elastic moduli of porous rocks:Low-frequency limit. Geophyslcs 50 (12), 2797–2807.
Vitale, G., Greco, L., Alessandro, A.D., Scudero, S., 2018. Bandwidth extension of a 4.5 Hz geophone for seismic monitoring purpose. In: 2018 IEEE International Conference on Environmental Engineering (EE).
Wojcik, K.M., Espejo, I.S., Kalejaiye, A.M., et al., 2016. Bright spots, dim spots: geologic controls of direct hydrocarbon indicator type, magnitude, and detectability. Niger Delta Basin: Interpretation 4 (3), SN45–SN69. https://doi.org/10.1190/INT-2016-0062.1.
Wu, J., Wu, G., Zong, Z., 2015. Attenuation of P waves in a porous medium containing various cracks. Chin. J. Geophys. Ed. 58 (4), 1378–1389. https://doi.org/10.6038/cjg20150424.
Yin, X.-Y., Deng, W., Zong, Z.-Y., 2016. AVO inversion based on inverse operator estimation in trust region. J. Geophys. Eng. 13 (2), 194–206.
Yin, X., Zhang, S., 2014. Bayesian inversion for effective pore-fluid bulk modulus based on fluid-matrix decoupled amplitude variation with offset approximation. Geophysics 79 (5), R221–R232. https://doi.org/10.1190/geo2013-0372.1.
Yu, A.-B., Standish, N., McLean, A., 1993. Porosity calculation of binary mixtures of nonspherical particles. J. Am. Ceram. Soc. 76 (11), 2813–2816. https://doi.org/10.1111/j.1151-2916.1993.tb04021.x.
Zdanowski, P., Górniak, M., 2014. Dim and bright spots as indicators of the Zechstein Main Dolomite hydrocarbon reservoir in Poland. Interpretation 2 (4), SP17–SP30. https://doi.org/10.1190/INT-2014-0039.1.
Zhang, L., Qi, J., Zhang, K., et al., 2019. Calibrate complex fracture model for subsurface flow based on Bayesian formulation. Petrol. Sci. 16 (5), 1105–1120. https://doi.org/10.1007/s12182-019-00357-5.
Zhang, Y., Liu, H., Cui, D., et al., 2016. Construction and application of the Russell fluid factor with squirt flow effect. Chin. J. Geophys. 59 (10), 3901–3908. https://doi.org/10.6038/cjg20161033 (in Chinese).
Zhang, Y., Jin, Z., Chen, Y., et al., 2018. Pre-stack seismic density inversion in marine shale reservoirs in the southern Jiaoshiba area, Sichuan Basin, China. Petrol. Sci. 15 (3), 484–497. https://doi.org/10.1007/s12182-018-0242-1 (in Chinese).
Zong, Z., Li, K., Yin, X., et al., 2017. Broadband seismic amplitude variation with offset inversion. Geophysics 82 (3), M43–M53. https://doi.org/10.1190/geo2016-0306.1.
Zong, Z., Yin, X., Wu, G., 2015. Geofluid discrimination incorporating poroelasticity and seismic reflection inversion. Surv. Geophys. 36 (5), 659–681. https://doi.org/10.1007/s10712-015-9330-6.
Zong, Z., Wang, Y., 2019. Amplitude variation with angle inversion for fluid discrimination with the consideration of squirt flow. SEG Technical Program Expanded Abstracts 2019 734–738.
Zong, Z., Wang, Y., Li, K., et al., 2018. Broadband seismic inversion for low-frequency component of the model parameter. IEEE Trans. Geosci. Rem. Sens. 56 (9), 5177–5184. https://doi.org/10.1109/TGRS.2018.2810845.
Zoeppritz, K., Erdbebenwellen VIII, B., 1919. On the reflection and penetration of seismic waves through unstable layers. Göttinger Nachrichten 1, 66–84.